THE JOURNAL OF PHYSICAL CHEMISTRY A

Article

pubs.acs.org/JPCA

Neutral-Fragmentation Paths of Methane Induced by Intense Ultrashort IR Laser Pulses: Ab Initio Molecular Orbital Approach

Shiro Koseki,[†,‡] Noriyuki Shimakura,[§] Yoshiaki Teranishi,[∥,#] Sheng Hsien Lin,[⊥,∇] and Yuichi Fujimura*[,∇,○]

[†]Department of Chemistry, Graduate School of Science, and [‡]The Research Institute for Molecular Electronic Devices (RIMED), Osaka Prefecture University, 1-1 Gakuen-cho, Naka-ku, Sakai 599-8531, Japan

[§]Department of Chemistry, Niigata University, Ikarashi Nino-cho 8050, Niigata 950-2181, Japan

[∥]Physics Division, National Center for Theoretical Sciences, Hsin-Chu, 300 Taiwan

[#]Department of Applied Chemistry, Institute of Molecular Science, and [⊥]Institute of Physics, National Chiao-Tung University, Hsin-Chu, 300 Taiwan

[∇]Institute of Atomic and Molecular Science, Academia Sinica, Taipei 10617, Taiwan

[○]Department of Chemistry, Graduate School of Science, Tohoku University, Sendai 980-8578, Japan

ABSTRACT: Instantaneous (laser-field-dependent) potential energy curves leading to neutral fragmentations of methane were calculated at several laser intensities from 1.4×10^{13} to 1.2×10^{14} W/cm^2 (from 1.0×10^{10} to 3.0×10^{10} V/m) using ab initio molecular orbital (MO) methods to validate the observation of neutral fragmentations induced by intense femtosecond IR pulses (Kong et al. *J. Chem. Phys.* **2006**, *125*, 133320). Two fragmentation paths, $CH_2 + 2H$ and $CH_2 + H_2$, in $^1T_2$ superexcited states that are located in the energy range of 12−16 eV were considered as the reaction paths because these states are responsible for Jahn−Teller distortion opening up reaction paths during ultrashort pulses. As field intensity increased, the low-lying excited $^1A_1$ states originated from the Jahn−Teller $^1T_2$ states were substantially stabilized along the neutral-fragment path $CH_4 \rightarrow CH_2 + 2H$ and were located below the ionization threshold. On the other hand, the low-lying excited $^1B_1$ states, which also originate from the Jahn−Teller $^1T_2$ states, were embedded on the ionized state along the dissociation path to $CH_2 + H_2$. This indicates that ionic fragments, rather than neutral ones, are produced along the $CH_2 + H_2$ path. The computational results support neutral fragmentations through superexcited states proposed by Kong et al.

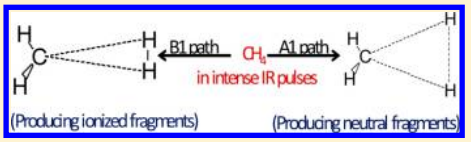

1. INTRODUCTION

Chemical reactions induced by intense laser pulses beyond the so-called multiphoton regime have attracted considerable attention.[1−3] Several mechanisms for intense-field chemical reactions have been proposed to explain mass spectra of positively charged fragments. The proposed mechanisms include Coulomb explosion,[4] charge migration,[5] charge resonance-enhanced ionization and dissociation,[6] multielectron dissociative ionization,[7] field-assisted dissociation mechanisms,[8] and nonadiabatic dynamics of electronic degrees of freedom.[9]

Kong et al.[10] reported experimental results for methane irradiated by intense ultrashort (40 fs) IR (800 mn) laser pulses. A notable finding was that neutral fragments, CH and H, were produced in addition to ionic fragments. The neutral fragments were clarified by observation of fluorescence from their electronically excited states. The fluorescence revealed a nonlinear dependence on laser intensity, namely, (10 ± 1)-photon processes involved before the laser intensity reached 2×10^{14} W/cm^2. Furthermore, the CH radical fragments in electronic excited states ($A^2\Delta$, $B^2\Sigma^-$, and $C^2\Sigma^+$) were observed to be vibrationally and rotationally hot. Evidence of the production of rotationally hot CH fragments suggests a two-step model, $CH_4 \rightarrow CH_2 \rightarrow CH$, because of asymmetric dissociation.[10] On the basis of the energy diagram of CH_4 under field-free conditions, Kong et al.[10] explained their experimental results and proposed a multiple-channel dissociation through superexcited states of the parent molecule as the neutral-fragmentation model. In relation to the mechanism of neutral fragmentations, Azarm et al.[11] reported the direct observation of superexcited states in methane using a pump−probe technique with a pulse duration of about 50 fs (full width at half-maximum). A depletion of the CH ($A^2\Delta \rightarrow X^2\Pi$) fluorescence signal of the delay time was attributed to the de-excitation of superexcited states by the probe pulse. The lifetime of the superexcited state was measured to be in the range of 50−160 fs.

Concerning the nonlinear dependence on laser intensity, Teranishi et al.[12] presented a theoretical interpretation based on Floquet treatment. They assumed that the fluorescence intensity of CH radicals is proportional to the excitation probability of methane. The idea of their theoretical treatment was based on the fact that valence excited states of methane are energetically close to Rydberg states or buried in the manifold of Rydberg states. In other words, a dense state manifold

Received: October 8, 2012
Revised: December 6, 2012
Published: December 12, 2012

includes many electronic states, and resonant coupling with IR laser fields is assumed to occur and to create Floquet states before the electronic transition from the ground state. The transition from the ground state to valence excited states can be described by a first-order dipole approximation.

To our knowledge, there are no theoretical explanations for why superexcited states participate in the production of neutral fragments of methane induced by intense femtosecond laser pulses. Although the role of superexcited states in photodissociation under field-free conditions has been investigated in detail,[13−19] the treatment of superexcited states under field-free conditions cannot be used under conditions of intense ultrashort IR laser pulses.

This article focuses on how the potentials of superexcited states of methane behave in intense laser fields. For this purpose, we used a field-dependent ab initio MO approach that has been successfully applied to the explanation of potential deformations and fragmentations of CO_2.[20,21] We took into account the effects of vibrational motions in optically active states in the early stage of photofragmentation of methane during irradiation of ultrashort pulses. In this early stage, the Jahn−Teller effect in $^1T_2$ superexcited states opens channels to the neutral-fragmentation paths, $CH_2 + 2H$ and $CH_2 + H_2$. In the next section, theoretical basis and procedures used in the present investigation are briefly described. In section 3, ab initio MO results are discussed with respect to instantaneous potential energy curves (PECs) along the neutral-fragmentation paths for $CH_2 + H_2$ and $CH_2 + 2H$ under an electric field of $E = 10^9-10^{10}$ V/m ($10^{12}-10^{14}$ W/cm^2). Finally, a qualitative discussion is provided on the nuclear dynamics producing neutral fragments through such superexcited states.

2. THEORETICAL TREATMENTS

2a. Reaction Paths for Neutral Fragmentations, $CH_2 + 2H$ and $CH_2 + H_2$. In most theories of fragmentations induced by intense femtosecond pulses, vibrational motions are frozen during the femtosecond duration of the laser pulse. This is called the frozen-nuclei approximation. It should be noted that this approximation cannot be applied to the methane fragmentation experiments of Kong et al.[10] for the following two reasons: First, the oscillation periods for the H−C−H bending mode (1369 cm^{-1}) and the C−H stretching mode (3036 cm^{-1}) in the ground state, calculated to be 24 and 11 fs, respectively, are explicitly shorter than the pulse duration (40 fs) used in their experiments.[10] Second, the bending and stretching vibrational modes belonging to the t_2 representation are Jahn−Teller modes. It is well recognized that the T_d structure of methane is deformed by the Jahn−Teller effect.[22,23] When the molecule is promoted from the ground state to a $^1T_2$ excited state, there are four Jahn−Teller modes ($t_2 \times t_2 = a_1 + e + t_1 + t_2$). An a_1 mode does not provide any geometrical distortion, and there is no t_1 motion in methane. An e mode provides D_{2d} structures, whereas a t_2 mode provides C_{2v} structures. Linear combinations of the t_2 stretching mode can provide one long C−H bond and derive the dissociation into $CH_3 + H$.[23a] Linear combinations of the t_2 bending and stretching modes can correlate with the dissociations

$$CH_4 \rightarrow CH_2 + 2H \tag{1a}$$

and

$$CH_4 \rightarrow CH_2 + H_2 \tag{1b}$$

Along this t_2 deformation, the $^1T_2$ excited state splits into three states within C_{2v} symmetry, namely, $^1A_1$, $^1B_1$, and $^1B_2$. Accordingly, the bending and stretching should play important roles in the early events of the reaction dynamics of methane. It is essential to investigate how the superexcited potentials along these vibrational coordinates change under intense laser-field pulses to clarify the neutral-fragmentation mechanisms of methane under intense ultrashort laser pulses. Because a superexcited state is embedded in the ionization manifold and even in the dissociation continuum of methane, the ionization processes would be more preferable than the neutral fragmentations if the shape of the potential energy surfaces of the superexcited states were not distorted markedly by the laser field.

The main configuration of the ground state ($^1A_1$) correlates not to that of the ground state at the dissociation limit, but to that of the lowest excited $^1A_1$ state at the dissociation limit. Accordingly, an avoided crossing should occur between the potential energy surfaces of the ground and lowest $^1A_1$ states. In other words, it is difficult to obtain a smooth PEC for the lowest excited $^1A_1$ state, if molecular orbitals are optimized only for the excited $^1A_1$ state. Therefore, it was decided that the geometry should be optimized for the ground state ($^1A_1$ in T_d) for the purpose of avoiding this difficulty. Then, as long as C_{2v} symmetry is maintained, the ground state correlates not to the ground state of $CH_2(^3B_1) + H_2$, but to that of $CH_2(^3B_1) + 2H(^2S)$.

On the other hand, the main configuration of the $^1B_1$ state correlates to $CH_4 \rightarrow CH_2 + H_2$, where the electronic state of CH_2 belongs to the B_1 representation and also correlates to the lowest $^1\Delta$ state of linear CH_2. The dissociation path for the lowest $^1B_1$ state into $CH_4 \rightarrow CH_2(^1B_1) + H_2(^1\Sigma_g^+)$ was already reported by Mebel et al.[24] Note that the dissociation path obtained for the lowest $^1B_2$ state is exactly the same as that obtained for the lowest $^1B_1$ state except that the dissociation direction is different; that is, it dissociates into $CH_2 + H_2$ or $H_2 + CH_2$. In the present article, the fragmentation path $CH_4 \rightarrow CH_2 + 2H$ is called the A_1 path, and the fragmentation path $CH_4 \rightarrow CH_2 + H_2$ is called the B_1 path.

2b. Potential Energy Curves for Electronically Excited States in the Presence of Intense Laser Fields. The optical cycle (~2.6 fs) of an IR (800 nm) laser is much shorter than the pulse length (~40 fs) used in our experiments.[10] The electric field of the laser oscillates too fast for the nuclei to follow. The reactions induced by such an intense IR laser pulse can be described by an effective potential energy averaged over one optical cycle of the laser.[20,21] For example, the resultant effective potential energy $\bar{U}(R,t)$ of a diatomic molecule at time t can be expanded in terms of the pulse envelope, $f(t)$, as

$$\bar{U}(R, t) = U(R) - \frac{1}{4}\alpha(R) f^2(t) - \frac{2}{32}\gamma(R) f^4(t) + \cdots \tag{2}$$

where $U(R)$ is the field-free potential energy and $\alpha(R)$ and $\gamma(R)$ are the polarizability and hyperpolarizability, respectively, of the molecule. It should be noted that, under an intense laser field, the convergence in eq 2 is slow, and higher-order terms might make a significant contribution. Accordingly, eq 2 could not be employed in the present investigation, and configuration interaction (CI) calculations (variational methods) were performed to obtain instantaneous PECs of low-lying states when an electric field was applied. The magnitudes of the instantaneous potential energies can be regarded as the

Table 1. Vertical Excitation Energies and Corresponding Oscillator Strengths at the Energy Minimum of the Ground State (X^1A_1) with No Electric Field[a]

T_d	V (%)	ΔE (eV)	f_L[b]	f_V[b]	C_{2v}[c]	ΔE (eV)	f_L[b]	f_V[b]
X^1A_1	97	0			X^1A_1	0		
1^1T_2	23	11.18	0.471	0.480	1^1A_1	10.11	0.022	0.016
($t_2 \rightarrow a_1^*$)					1^1B_1 (B_2)	8.24	0.065	0.106
2^1T_2	14	12.58	0.046	0.066	2^1A_1	12.32	0.168	0.068
($t_2 \rightarrow t_2^*$)					2^1B_1 (B_2)	11.00	0.007	0.002
1^1T_1	16	12.68	0	0	3^1B_1 (B_2)	12.01	0.002	0.000
($t_2 \rightarrow t_2^*$)								
1^1E	11	12.69	0	0	3^1A_1	14.14	0.122	0.048
($t_2 \rightarrow t_2^*$)								
1^1A_1	2	12.98	0	0	4^1A_1	15.65	0.244	0.244
($t_2 \rightarrow t_2^*$)								
2^1T_1	11	13.63	0	0	4^1B_1 (B_2)	12.47	0.003	0.001
2^1E	9	13.83	0	0	5^1A_1	16.48	0.017	0.011
2^1A_1	3	14.06	0	0	6^1A_1	17.11	0.000	0.001
3^1T_2	9	14.20	0.004	0.001	7^1A_1	17.39	0.001	0.003
($t_2 \rightarrow a_1^*$)					5^1B_1 (B_2)	13.42	0.000	0.000
4^1T_2	6	14.41	0.751	0.564	8^1A_1	17.98	0.062	0.038
($t_2 \rightarrow a_1^*$)					6^1B_1 (B_2)	14.03	0.350	0.212
3^1T_1	22	14.95	0	0	7^1B_1 (B_2)	16.79	0.007	0.005
5^1T_2	20	15.07	0.103	0.111	9^1A_1	18.04	0.053	0.025
($t_2 \rightarrow t_2^*$)					8^1B_1 (B_2)	17.10	0.064	0.042
3^1E	26	15.12	0	0	10^1A_1	18.45	0.012	0.014
($t_2 \rightarrow t_2^*$)								
4^1T_1	0	15.43	0	0	9^1B_1 (B_2)	17.70	0.002	0.002
6^1T_2	6	15.73	1.717	1.215	11^1A_1	18.72	0.100	0.092
					10^1B_1 (B_2)	18.24	0.036	0.038
3^1A_1	15	16.01	0	0	12^1A_1	18.84	0.094	0.063
($t_2 \rightarrow t_2^*$)								

[a]A T_1 state at a T_d structure is split into A_2, B_1, and B_2 sates at a C_{2v} structure, and a T_2 state at a T_d structure is split into A_1, B_1, and B_2 states at a C_{2v} structure. An E state at a T_d structure is split into A_1 and A_2 states at a C_{2v} structure, and an A_1 state correlates to an A_1 state at a C_{2v} structure. This table includes only A_1 and B_1 states at a C_{2v} structure. V (%) denotes weights of the configuration state functions consisting only of active orbitals, where many excitations from the active orbitals to the external orbitals are included in the MCSCF calculations followed by FOCI calculations (MCSCF + FOCI). When C_{2v} symmetry is used, the numbers of configuration state functions included in MCSCF + FOCI calculations are 77100 ($^1A_1$), 75504 ($^1A_2$), 76284 ($^1B_1$), 76284 ($^1B_2$), 120104 ($^3A_1$), 119456 ($^3A_2$), 119788 ($^3B_1$), and 119788 ($^3B_2$). [b]f_L is the oscillator strength computed using the length form of the transition moment $\langle X^1A_1|r|\text{state}\rangle$, whereas f_V is that computed by using the velocity form of transition moment $\langle X^1A_1|\partial/\partial r|\text{state}\rangle$. [c]The first five columns indicate the results at the T_d structure optimized for the ground state, whereas the last four columns indicate the results at the C_{2v} structure. For all $^1A_1$ states listed in the last four columns, the optimized geometry for the lowest excited $^1A_1$ state was used (not the ground state), whereas the optimized geometry for the lowest excited $^1B_1$ ($^1B_2$) state was used for all $^1B_1$ ($^1B_2$) states listed in these columns. Because the transition is forbidden from the ground state to a $^1A_2$ state, the geometry optimization was not performed for the lowest $^1A_2$ state, and no results are shown for A_2 states.

maximum magnitude of the effective potential energies at each point along the dissociation paths.

For practical evaluation of instantaneous PECs, the fully optimized reaction space multiconfiguration self-consistent field (MCSCF) method was employed together with Dunning's aug-cc-pVTZ basis set.[25−27] The MCSCF active space includes all valence orbitals and electrons. Under field-free conditions, the MOs and expansion coefficients of configuration state functions (CSFs) were optimized by the MCSCF method. After the optimization procedure, the relative energies of low-lying electronic states and the transition dipole moments between the ground state and low-lying states were refined using the first-order configuration interaction (FOCI) method.[25,28] When an electric field was applied, zero-field MOs were simply used in the FOCI calculations, in which the molecular orbitals were not optimized. All of the MO calculations were performed using the GAMESS suite of program codes.[25]

3. RESULTS AND DISCUSSION

It is well recognized that the two energy ranges of 11−16 and 18−24 eV are of interest for superexcited states under field-free conditions.[19] The superexcited states in the lower-energy range have a single electron hole in the highest occupied molecular orbital (HOMO) ($1t_2$) [denoted by$(1t_2)^{-1}$], whereas those in the higher-energy range have a single electron hole in the next HOMO ($2a_1$) [denoted by $(2a_1)^{-1}$]. We restrict ourselves to the excited $^1T_2$ states in the low-energy range of 11−16 eV.

Table 1 lists the vertical excitation energies from the ground state to low-lying states in methane (T_d), together with the weight factors of valence character and the oscillator strengths under field-free conditions. The geometrical structure was optimized for the ground state ($^1A_1$). Note that, at the present level of theory, the vertical and adiabatic ionization energies (IEs) were calculated to be 13.11 and 11.60 eV, respectively.[29] It should be noted that only 1^1T_2 and 2^1T_2 are optically active in the neighborhood of the ionization threshold for the T_d structure. Table 1 also includes the excitation energies and the

dx.doi.org/10.1021/jp309931c | J. Phys. Chem. A 2013, 117, 333−341

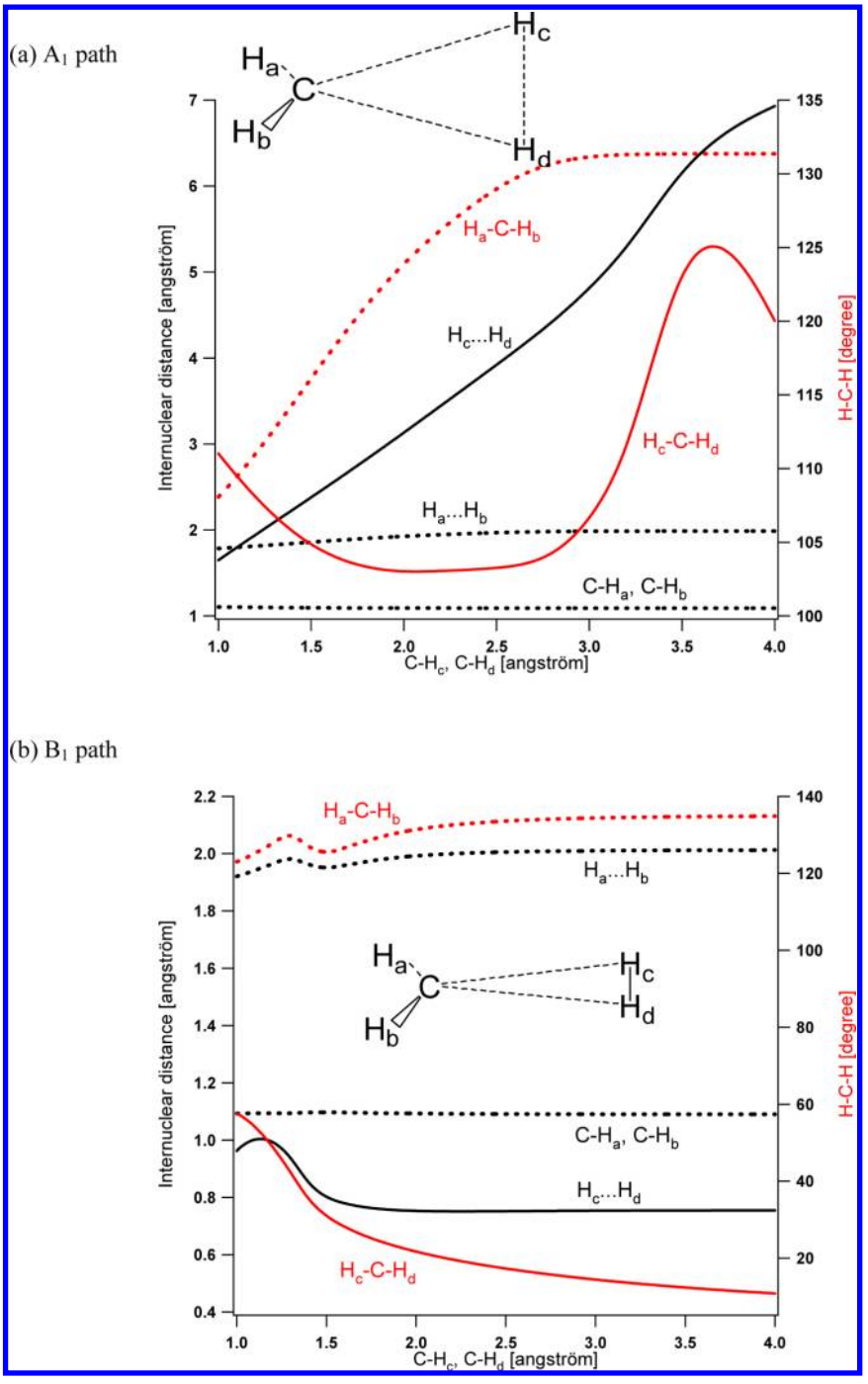

Figure 1. Dissociation paths optimized for the (a) ground state ($^1A_1$) and (b) lowest $^1B_1$ state in the absence of an electric field. Black lines are for distances (left vertical axis), and red lines are for angles (right vertical axis). Solid lines are for leaving hydrogen atoms, and broken lines are for CH_2 fragments.

corresponding oscillator strengths after geometry deformation from the T_d structure to the C_{2v} structures optimized for the lowest excited $^1A_1$ and the lowest $^1B_1$ states.

According to the present MCSCF + FOCI calculations, the valence character of the lowest $^1T_2$ state (1^1T_2) originates from the singly excited configuration generated by the HOMO−LUMO (lowest unoccupied molecular orbital) transition ($t_2 \rightarrow a_1^*$). The valence characters of the next lowest four states (2^1T_2, 1^1T_1, 1^1E, and 1^1A_1) originate from the singly excited configuration generated by the HOMO−next LUMO ($t_2 \rightarrow t_2^*$) transition, where only the 2^1T_2 state corresponds to a dipole-allowed optical transition in the frozen-nuclei approximation. As shown in Table 1, the weight factors of valence character are below 50% and suggest that strong mixing of valence and Rydberg characters occurs in low-lying excited states in methane. Therefore, it seems meaningless to classify the states into valence and Rydberg categories.

Figure 1 shows two fragmentation paths, A_1 and B_1, as introduced in section 2b. The C−H bond length for the leaving hydrogen atoms (H_c and H_d) is taken as the abscissa. At every point of the abscissa, the other geometrical parameters were optimized within C_{2v} symmetry. On the PEC of the ground

dx.doi.org/10.1021/jp309931c | J. Phys. Chem. A 2013, 117, 333−341

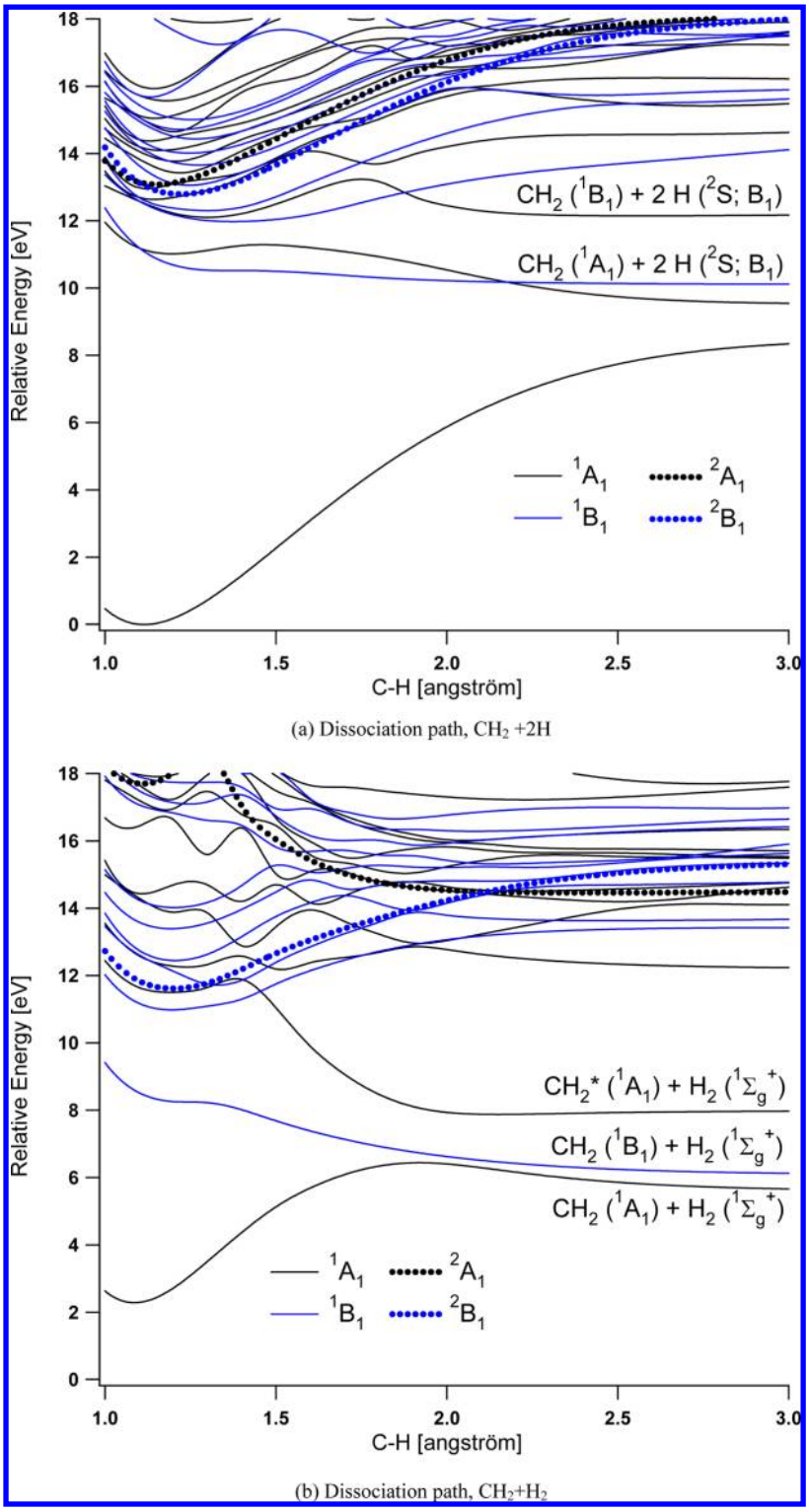

Figure 2. Dissociation potential energy curves (PECs) of low-lying $^1A_1$ and $^1B_1$ states with no electric field along the (a) A_1 and (b) B_1 paths (see text). The energy zero is set to the ground-state energy at its optimized geometry. Note that the energies of the low-lying $^1A_2$ and $^1B_2$ states are not shown.

state, the $H_c\cdots H_d$ distance increased as the C−H_c bond length (and the C−H_d bond length) increased (see Figure 1a), which indicates that the dissociation limit must be CH_2 + 2H. On the other hand, $H_c\cdots H_d$ stays short on the PEC of the lowest $^1B_1$ state even at the dissociation limit, which indicates that the dissociation limit must be CH_2 + H_2. At the optimized geometry for the ground state ($^1A_1$), all H−C−H angles are 109.5°, and all C−H bond lengths are 1.101 Å. At the optimized geometry for the lowest $^1B_1$ state, the geometry has C_{2v} symmetry, and its geometrical parameters are C−H_a = C−H_b = 1.094 Å, H_a−C−H_b = 128.5°, C−H_c = C−H_d = 1.227 Å, and H_c−C−H_d = 47.2° (see Figure 1). These values are very similar to those reported by Mebel et al.[28]

dx.doi.org/10.1021/jp309931c | J. Phys. Chem. A 2013, 117, 333−341

Figure 2 shows PECs of the low-lying singlet states along the A_1 and B_1 paths shown in Figure 1, together with those of a few low-lying doublet states in the ionized species in the absence of an electric field. The vertical IE $CH_4(^1A_1) \rightarrow CH_4^+(^2T_2) + e^-$ was calculated to be 13.11 eV (MCSCF + FOCI), whereas the adiabatic IEs to $CH_4^+(^2A_1)$ and to $CH_4^+(^2B_1)$ were calculated to be 11.64 and 11.60 eV, respectively.[23c] Additionally, $CH_4^+(^2B_2)$ has the same structure as $CH_4^+(^2B_1)$ except for a 90° rotation with respect to the principle axis of C_{2v} symmetry. The PECs along the B_1 path (Figure 2b) are basically the same as those reported by Mebel et al.[24]

Nonzero oscillator strengths between the ground state and the relevant excited states are required as one of the necessary conditions for the photodissociation of methane in an intense laser field.[12,30] Along the A_1 path, where the geometrical symmetry is deformed from T_d to C_{2v}, the third and fourth excited $^1A_1$ states have relatively large oscillator strengths (f_L or f_V), and the sixth $^1B_1$ state has a large oscillator strength at the structure optimized for the lowest $^1B_1$ state (see the right three columns of Table 1 and the footnotes to Table 1). These states are labeled 3^1A_1, 4^1A_1, and 6^1B_1 in Table 1. These excited states can be recognized as superexcited states, because their energies are higher than the IEs under field-free conditions. In fact, when the molecular geometry is deformed into C_{2v} symmetry, the excitation energies to these excited states from the energy minimum (T_d) of the ground state are estimated to be 14.14 eV (3^1A_1), 15.65 eV (4^1A_1) and 14.03 eV (6^1B_1), and their oscillator strengths are 0.122, 0.244, and 0.350, respectively.

Figure 3 shows instantaneous PECs for 3^1A_1 along the A_1 path shown in Figure 1, upon the application of electric fields (E), namely, $E = 0$, $\pm 1.54 \times 10^{10}$, and $\pm 3.09 \times 10^{10}$ V/m, where these values are 0, 0.03, and 0.06, respectively, in atomic units and also correspond to 0, $\pm 3.16 \times 10^{13}$, and $\pm 1.26 \times 10^{14}$ W/cm^2. When the direction of the electric field is parallel (antiparallel) to the direction of the z axis as illustrated at the top of Figure 3, the value of the electric field is defined as positive (Figure 3a) [negative (Figure 3b)]. The instantaneous PECs for the lowest ionized states, that is, the lowest $^2B_1$ and $^2A_1$ states in CH_4^+, which are denoted by thick red and green lines, respectively, are also depicted for comparison. Surprisingly, the instantaneous PECs for superexcited states were energetically pushed down along the A_1 path together and became shallower as the electric field increased. At $|E| = 0.06$ au, the PECs were lowered by about 4 eV compared with those at $E = 0$. This indicates a substantial increase in the probability of neutral fragmentation along the A_1 path as the laser intensity increased.

On the other hand, the energy lowering of the PESs of the lowest $^2B_1$ and $^2A_1$ states in CH_4^+ was ~1 eV when the electric field of the laser pulse was changed from $|E| = 0$ to $|E| = 0.06$ au and was small compared with that of the 3^1A_1 state along the A_1 path. This means that the neutral dissociation channel $CH_4 \rightarrow CH_2 + 2H$ is preferred to the channel $CH_4^+ \rightarrow CH_2^+ + 2H$ in intense fields. However, it does not mean that ionized fragments cannot appear. Several fragmentation paths exist in polyatomic molecules. For methane, another dissociation path, for example, $CH_4^+ \rightarrow CH_3^+ + H$, can be considered. In fact, experimentally, $CH_4^+ \rightarrow CH_3^+ + H$ is recognized as the possible primary reaction channel in intense fields, and furthermore, $CH_3^+ \rightarrow CH_2^+ + H$ and $CH_2^+ \rightarrow CH^+ + H$ are recognized as secondary reaction channels.[8] Thus, selection of the reaction channel at the initial stage is the key to which fragments, neutral or ionized ones, are produced for CH_4 dissociation in intense laser fields.

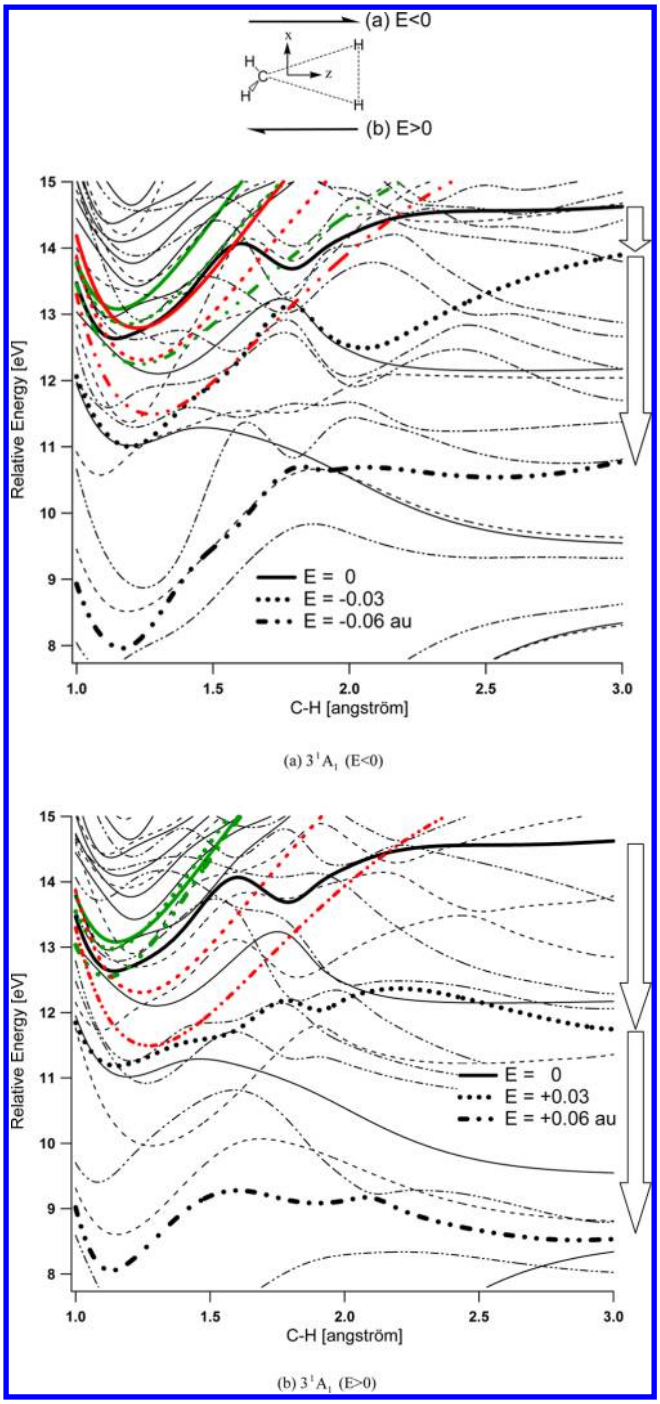

Figure 3. Instantaneous potential energy curves (PECs) of the third lowest excited $^1A_1$ state along the A_1 path. The target states are emphasized by thick black lines, and the red and green thick lines are for the ionized $^2B_1$ and $^2A_1$ states, respectively, in CH_4^+. Note that the $^2A_1$ state in CH_4^+ corresponds to the $^2B_2$ state (ground state) at the D_{2d} structure. The inset at the top of this figure depicts the directions of positive and negative electric fields.

Field-dependent behaviors in the instantaneous PECs similar to those shown in Figure 3 (i.e., the PECs along the A_1 path are pushed down) were also obtained for the 4^1A_1 state. This suggests that the characteristic feature in the PECs is not specific to the 3^1A_1 state but common to the $^1A_1$ states.

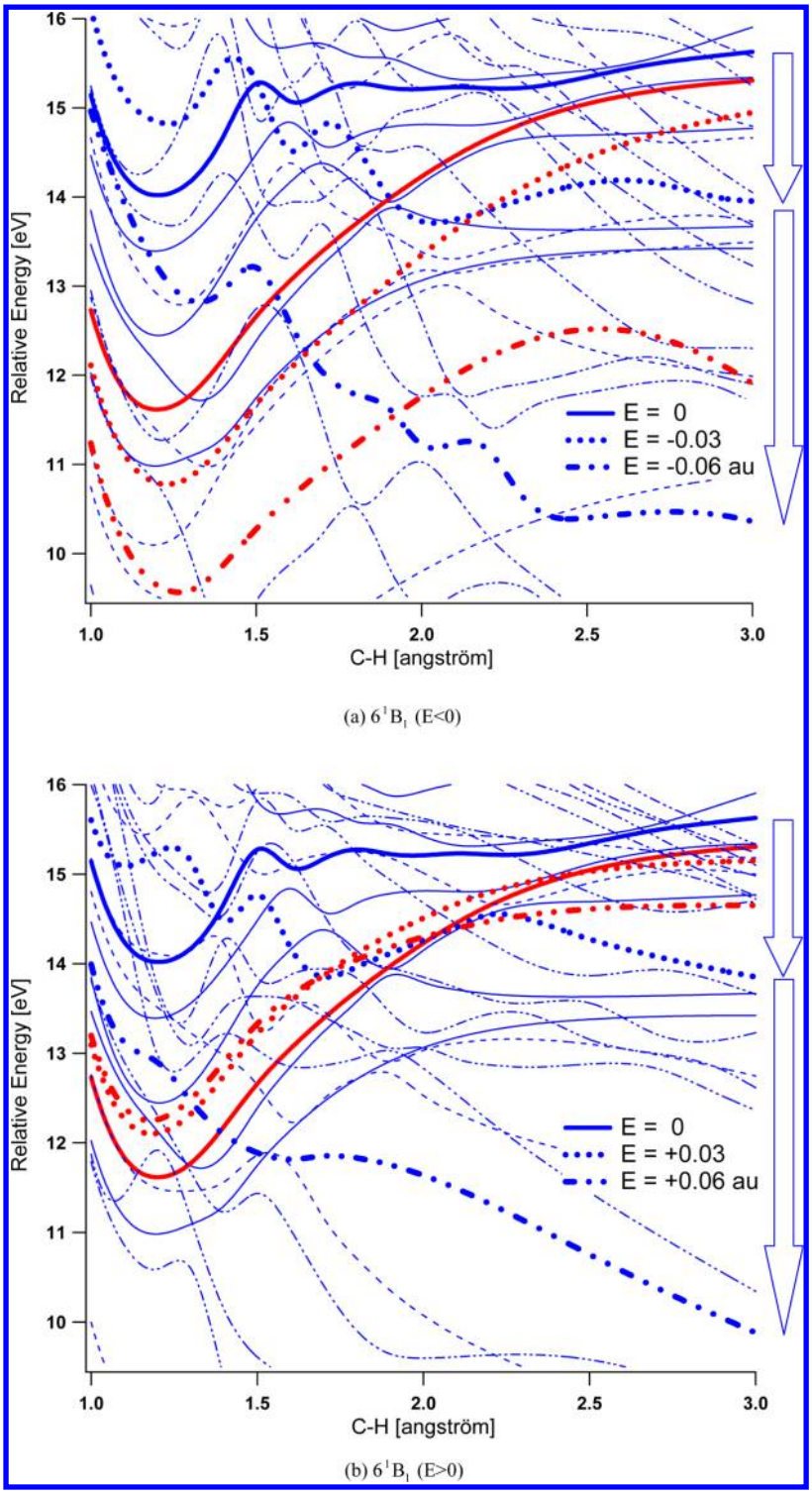

Figure 4. Instantaneous potential energy curves (PECs) of the sixth lowest $^1B_1$ state along the B_1 path. The target states are emphasized by thick blue lines, and the red thick lines are for the ionized states ($^2B_1$ state in CH_4^+).

Figure 4 shows calculated instantaneous PECs of 6^1B_1 along the B_1 path shown in Figure 1. In contrast to the results for the 3^1A_1 state along the A_1 path, the field dependence of the instantaneous PECs for 6^1B_1 is different; the instantaneous PEC along the B_1 path for 6^1B_1 is embedded on the PECs of the ionized states. This indicates that ionic fragments, rather than neutral ones, are produced along the B_1 path as a result of nonadiabatic couplings between the two channels $CH_4 \rightarrow CH_2 + H_2$ and $CH_4^+ \rightarrow CH_2^+ + 2H$. The calculated ab initio MO results shown in Figures 3 and 4 suggest that channel $CH_4 \rightarrow CH_2 + 2H$, not $CH_4 \rightarrow CH_2 + H_2$, is responsible for neutral fragmentation.

We now make a brief comment on the accuracy of the wave functions used in the MCSCF method. For field-free conditions, comparison of the oscillator strengths between the length and velocity forms, f_L and f_V, indicates considerably

dx.doi.org/10.1021/jp309931c | J. Phys. Chem. A 2013, 117, 333−341

accurate wave functions for the superexcited states in low-energy ranges because these two values agree with each other to the same order, as reported in Table 1. When exact wave functions are used for the ground and excited states, the same value must be obtained for both f_L and f_V. For nonzero fields, a detailed discussion about the reliability of the present MCSCF + FOCI calculations was published for the deformations and dissociations of CO_2, CO_2^+, and CO_2^{2+} under intense-laser-field conditions.[21] In that treatment, both the MOs and the expansion coefficients of the configuration state functions were optimized. A simplified method was adopted in the present work as described in the Theoretical Treatments section. Because the reliability of electronic wave functions decreases as the field strength increases, the instantaneous PECs of low-lying states were calculated under field strengths of $|E| = 0-0.06$ au. These calculated results show that the PECs provide consistent results on lowering or raising the field strength from 0 to 0.06 au, as illustrated in Figures 3 and 4. Therefore, the reliability of the present results is relatively high.

Finally, Kong et al.[10] proposed the two-step fragmentation mechanism $CH_4 \rightarrow CH_2 \rightarrow CH$ for CH_4 in intense laser fields. Although it is shown in this article that the neutral fragmentations take place in electronic excited states through A_1 path, quantum dynamical treatments based on multidimensional potential surfaces are necessary to confirm the fragmentation mechanism.[10] In the quantum dynamical treatment, two key issues have to be considered: nonadiabatic transition (NT) and intramolecular vibrational energy redistribution (IVR). As shown in Figure 3, many avoided crossings occur among the PECs along the A_1 path even below the ionization energy. This indicates that NT takes place among the time-dependent adiabatic states.[20,21,30] IVR plays an important role especially in electronic excited states. In the present treatment, vibrational modes of methane were restricted to Jahn–Teller-active modes, and multimode potential energy surfaces including other vibrational modes in electronic excited states have to be considered.

4. CONCLUSIONS

This article shows important roles of superexcited states for the neutral fragmentations of methane irradiated by ultrashort intense IR laser pulses (40 fs). Instantaneous PECs of superexcited states in the low-energy ranges were calculated using the field-dependent ab initio MO procedure. Instantaneous PECs along two neutral-fragmentation paths, $CH_4 \rightarrow CH_2 + 2H$ and $CH_4 \rightarrow CH_2 + H_2$, were considered taking into account vibrational modes leading to Jahn–Teller distortions. The electric field intensities generated by the pulses were set to $E = 0, \pm 3.16 \times 10^{13}$, and $\pm 1.26 \times 10^{14}$ W/cm^2. When methane is promoted to one of the superexcited $^1A_1$ states, it is predicted to dissociate as $CH_4 \rightarrow CH_2 + 2H$ along the A_1 path because these superexcited states are lower in energy than the ionized states near the Franck–Condon region. Therefore, it can be concluded that the probability of producing neutral fragments along this path increases as the intensity of the electric field of the laser increases. On the other hand, when methane is promoted to one of the superexcited $^1B_1$ states, it is predicted to dissociate as $CH_4 \rightarrow CH_2 + H_2$ along the B_1 path. However, these states are buried in the manifold of ionized states, and this path produces ions rather than neutral fragments. Quantum dynamical treatments of fragmentations through superexcited states with multidimensional potential energy surfaces should be the next stage in the present series of investigations. Finally, in this article, we concentrated on searching the neutral-fragmentation paths and omitted ionization processes. It should be noted that the evaluation of ionization rates during fragmentations is important because ionization is the main dynamic process of methane in intense ultrashort IR pulses.

AUTHOR INFORMATION

Corresponding Author

*E-mail: fujimurayuichi@m.tohoku.ac.jp.

Notes

The authors declare no competing financial interest.

ACKNOWLEDGMENTS

Y.F. thanks NSC (National Science Council) of Taiwan and JSPS (Japan Society for Promotion of Science) for his financial support.

REFERENCES

(1) Yamanouchi, K. *Science* **2002**, *295*, 1659–1660.
(2) Bandrauk, A. D., Gordon, R. J., Fujimura, Y., Eds. *Laser Control and Manipulation of Molecules*; ACS Symposium Series; American Chemical Society: Washington, D.C., 2002; Vol. *821*.
(3) Kono, H.; Sato, Y.; Tanaka, N.; Kato, T.; Nakai, K.; Koseki, S.; Fujimura, Y. *Chem. Phys.* **2004**, *304*, 203–226.
(4) Fransinski, L. J.; Colding, K.; Hatherly, P.; Baa, J.; Ross, I. N.; Toner, W. T. *Phys. Rev. Lett.* **1987**, *58*, 2424–2427.
(5) Mathur, D.; Safvan, C. P.; Kumar, G. R.; Krishnamurthy, M. *Phys. Rev. A* **1994**, *50*, R7–R9.
(6) Chelkowiski, S.; Conjusteau, A.; Zuo, T.; Bandrauk, A. D. *Phys. Rev. A* **1996**, *54*, 3235–3244.
(7) Hering, Ph.; Cornaggia, C. *Phys. Rev. A* **1998**, *57*, 4572–4580.
(8) Wang, S.; Tang, X.; Gao, L.; Elshakre, M.; Kong, E. F. *J. Phys. Chem. A* **2003**, *107*, 6123–6129.
(9) Markevitch, A. N.; Smith, S. M.; Romanov, D. A.; Schlegel, H. B.; Ivanov, M. Y.; Levis, R. J. *Phys. Rev. A* **2003**, *68*, 011402–1–011402–8.
(10) Kong, F.; Luo, Q.; Xu, H.; Sharifi, M.; Song, D.; Chin, S. L. *J. Chem. Phys.* **2006**, *125*, 133320-1–133320-5.
(11) Azarm, A.; Xu, H. L.; Kamali, Y.; Bernhardt, J.; Song, D.; Xia, A.; Teranishi, Y.; Lin, S. H.; Kong, F.; Chin, S. L. *J. Phys. B: At. Mol. Opt. Phys.* **2008**, *41*, 225601.
(12) Teranishi, Y.; Hayashi, M.; Kong, F.; Chin, S. L.; Chao, S. D.; Mineo, H.; Lin, S. H. *Mol. Phys.* **2008**, *106*, 333–339.
(13) Mitsuke, K.; Suzuki, S.; Imamura, T.; Koyano, I. *Chem. Phys.* **1991**, *94*, 6003–6006.
(14) Mordaunt, D. H.; Lambert, I. R.; Morley, G. P.; Ashford, M. N. R.; Dixon, R. N.; Western, C. M.; Schnieder, L.; Welge, K. H. *J. Chem. Phys.* **1993**, *98*, 2054–2065.
(15) Au, J. W.; Copoper, G.; Burton, G.; Olney, R. T. N.; Brion, C. E. *Chem. Phys.* **1993**, *173*, 209–239.
(16) Wang, J.-H.; Liu, K. *J. Chem. Phys.* **1998**, *109*, 7105–7112.
(17) Wang, J.-H.; Liu, K.; Min, Z.; Su, H.; Bersohn, R.; Preses, J.; Larese, J. Z. *J. Chem. Phys.* **2000**, *113*, 4146–4152.
(18) Kameta, K.; Kouchi, N.; Ukai, M.; Hatano, Y. *J. Electron Spectrosc. Relat. Phenom.* **2002**, *123*, 225–238.
(19) Kato, M.; Kameta, K.; Odagiri, T.; Kouchi, N.; Hatano, Y. *J. Phys. B: At. Mol. Opt. Phys.* **2002**, *35*, 4383–4400.
(20) Sato, Y.; Kono, H.; Koseki, S.; Fujimura, Y. *J. Am. Chem. Soc.* **2003**, *125*, 8019–8031.
(21) Kono, H.; Koseki, S.; Shiota, M.; Fujimura, Y. *J. Phys. Chem. A* **2001**, *105*, 5627–5636.
(22) Jahn, H. A.; Teller, E. *Proc. R. Soc. A* **1937**, *161*, 220–235.
(23) (a) Rabalais, J. W.; Bergmark, T. L.; Werme, O.; Karlsson, L.; Siegbahn, K. *Phys. Scr.* **1971**, *3*, 13–18. (b) The low-frequency t_2 mode has H–C–H bending motions and provides C_{2v} structures, even though ref 23a does not describe this deformation. In fact, the Jahn–Teller distortion of the D_{2d} structure can derive C_{2v} structures, as

described in Ref 23c. (c) As described in Ref 23a, the ground state in methane cation CH_4^+ is $^2T_2$ at the optimized T_d structure. The $^2T_2$ state is split into $^2B_2$ and ^2E states at the D_{2d} structure. The $^2B_2$ and ^2E states belong to A_1, B_1, and B_2 representations in the C_{2v} subgroup, and the $^2B_2$ state is the ground state. The Hessian matrix of the $^2B_2$ state ($^2A_1$ state in C_{2v} symmetry; see Figures 3 and 4) has two imaginary frequencies. The corresponding vibrational motions provide two identical C_{2v} structures, and their ground states are $^2B_1$ and $^2B_2$. The $^2B_1$ and $^2B_2$ states provide the same results (see the text). The Hessian matrices for the $^2B_1$ and $^2B_2$ states are positive-definite.

(24) Mebel, A. M.; Lin, S. H.; Chang, C.-H. *J. Chem. Phys.* **1997**, *106*, 2612−2620.

(25) Schmidt, M. W.; Baldridge, K. K.; Boatz, J. A.; Elbert, S. T.; Gordon, M. S.; Jensen, J. H.; Koseki, S.; Matsunaga, N.; Nguyen, K. A.; Su, S.; Windus, T. L.; Dupuis, M.; Montgomery, J. A., Jr. *J. Comput. Chem.* **1993**, *14*, 1347−1363.

(26) (a) Ruedenberg, K.; Schmidt, M. W.; Dombek, M. M.; Elbert, S. T. *Chem. Phys.* **1982**, *71*, 41−46; **1982**, *71*, 51−64; **1982**, *71*, 65−78. (b) Schmidt, M. W.; Gordon, M. S. *Annu. Rev. Phys. Chem.* **1998**, *49*, 233−266.

(27) (a) Dunning, T. H. J., Jr. *Chem. Phys.* **1989**, *90*, 1007−1023. (b) Kendall, R. A.; Dunning, T. H., Jr.; Harrison, R. J. *J. Chem. Phys.* **1992**, *96*, 6796−6806. (c) Basis Set Exchange. Pacific Northwest National Laboratory, Richland, WA, 2007; http://www.emsl.pnl.gov/forms/basisform.html.

(28) (a) Lengsfield, B. H. *J. Chem. Phys.* **1982**, *77*, 4073−4083. (b) Liao, D.-W.; Balasubramanian, K. *Chem. Phys. Lett.* **1993**, *213*, 174−180.

(29) Kong et al.[10] used IE = 12.6 eV. This value is for adiabatic ionization and can be found in: Berkowitz, J.; Greene, J. P.; Cho, H.; Ruscic, B. *J. Chem. Phys.* **1987**, *86*, 674−676. . The vertical IE is 13.6 eV (Bieri, G.; Asbrink, L. *J. Electron Spectrosc. Relat. Phenom.* **1980**, *20*, 149−167).

(30) Markevitch, A. N.; Romanov, D. A.; Smith, S. M.; Schlegel, H. B.; Ivanov, M. Y.; Levis, R. J. *Phys. Rev. A* **2004**, *69*, 013401-1−013401-13.